Published for SISSA by Springer

Received: June 21, 2022
Revised: October 25, 2022
Accepted: October 25, 2022
Published: November 14, 2022

Tri-resonant leptogenesis in a seesaw extension of the Standard Model

P. Candia da Silva, D. Karamitros, T. McKelvey and A. Pilaftsis

Department of Physics and Astronomy, University of Manchester, Manchester, M13 9PL, U.K.

E-mail: pablo.candiadasilva@manchester.ac.uk, dimitrios.karamitros@manchester.ac.uk, thomas.mckelvey@manchester.ac.uk, apostolos.pilaftsis@manchester.ac.uk

Abstract: We study a class of leptogenesis models where the light neutrinos acquire their observed small masses by a symmetry-motivated construction. This class of models may naturally include three nearly degenerate heavy Majorana neutrinos that can strongly mix with one another and have mass differences comparable to their decay widths. We find that such a tri-resonant heavy neutrino system can lead to leptonic CP asymmetries which are further enhanced than those obtained in the usual bi-resonant approximation. Moreover, we solve the Boltzmann equations by paying special attention to the temperature dependence of the relativistic degrees of freedom of the plasma. The latter results in significant corrections to the evolution equations for the heavy neutrinos and the lepton asymmetry that have been previously ignored in the literature. We show the importance of these corrections to accurately describe the dynamical evolution of the baryon-to-photon ratio η_B for heavy neutrino masses at and below 100 GeV, and demonstrate that successful leptogenesis at lower masses can be significantly affected by the variation of the relativistic degrees of freedom. The parameter space for the leptogenesis model is discussed, and it could be probed in future experimental facilities searching for charged lepton flavour violation and heavy neutrinos in future Z-boson factories.

Keywords: Baryo-and Leptogenesis, Sterile or Heavy Neutrinos, Neutrino Mixing, Early Universe Particle Physics

ArXiv ePrint: 2206.08352

https://doi.org/10.1007/JHEP11(2022)065

JHEP11(2022)065

Contents

1 Introduction

Observations done by the Wilkinson Microwave Anisotropy Probe (WMAP) and the Planck observatory indicate that the extent of the Baryon Asymmetry of the Universe (BAU) amounts to [1, 2]

$$\eta_B^{\text{CMB}} = 6.104 \pm 0.058 \times 10^{-10}. \tag{1.1}$$

Hence, explaining the observed BAU has been one of the central themes of Particle Cosmology for decades. The existence of this non-zero BAU is one of the greatest pieces of evidence for physics beyond the Standard Model (SM). In the SM, the neutrinos are strictly massless,

JHEP11(2022)065

and so this runs contrary to the observations of neutrino oscillations [3–5], which only exist for massive neutrinos. A minimal resolution to this problem will be to include additional heavy neutrinos which are singlets under the SM gauge group: $\mathrm{SU}(3)_c \times \mathrm{SU}(2)_L \times \mathrm{U}(1)_Y$. These additional neutrinos are permitted to have large masses due to the inclusion of a Majorana mass term which violates lepton number, L, by two units. They also provide a mechanism to render the SM neutrinos massive, whilst ensuring that the generated mass is small in scale through the famous seesaw mechanism [6–9]. On the other hand, the spacetime expansion of the FRW Universe provides a macroscopic arrow of cosmic time t, as well as Sakharov's necessary out-of-thermal equilibrium condition [10] needed to potentially generate a large lepton-number asymmetry. This asymmetry is then rapidly converted into a baryon asymmetry through $(B+L)$-violating sphaleron transitions while the temperature of the Universe remains above the temperature $T_{\rm sph} \approx 132\,\mathrm{GeV}$, after which these sphaleron transitions become exponentially suppressed. This mechanism is commonly referred to as *leptogenesis* [11].

A particularly interesting framework of leptogenesis is *Resonant Leptogenesis* (RL) [12, 13], which permits Majorana mass scales far lower than those that occur in typical Grand Unified Theory (GUT) models of leptogenesis [11, 14]. In RL models, the CP violation generated is greatly enhanced through the mixing of nearly degenerate heavy Majorana neutrinos N_α, provided

$$\left| m_{N_\alpha} - m_{N_\beta} \right| \sim \frac{\Gamma_{N_{\alpha,\beta}}}{2}\,,$$

where m_{N_α} and Γ_{N_α} are the masses and the decay widths of N_α, respectively. This mass arrangement in turn permits the generation of appreciable BAU at sub-TeV masses [12, 15], in agreement with neutrino oscillation parameters [13, 16].

In this paper we study a class of leptogenesis models that may naturally include three nearly degenerate heavy Majorana neutrinos which can strongly mix with one another and have mass differences comparable to their widths. We compute the leptonic CP asymmetries generated in such a tri-resonant heavy neutrino system, to find that their size is further enhanced in comparison to those that were naively determined in the usually considered bi-resonant approximation. Accordingly, this enhanced mechanism of leptogenesis will be called Tri-Resonant Leptogenesis (TRL). In the context of models realising TRL, our aim is to find neutrino Yukawa couplings whose size lies much higher than the one expected from a typical seesaw scenario, whilst still achieving the observed BAU. To this end, we solve the Boltzmann equations (BEs) that describe the evolution of heavy neutrino and lepton-asymmetry number densities before the sphaleron freeze-out temperature, after including decay and scattering collision terms. An important novelty of the present study is to assess the significance of the temperature dependence of the relativistic degrees of freedom (dofs) in the plasma. Finally, we analyse observables of charged Lepton Flavour Violation (cLFV) that could be tested in current and projected experiments, such as $\mu \to eee$ at Mu3e [17], $\mu \to e\gamma$ at MEG [18, 19], coherent $\mu \to e$ conversion at COMET [20] and PRISM [21], as well as matching the observed light neutrino mass constraints [3–5].

In our analysis we will not specify the origin of the structure of the Majorana-mass and the neutrino Yukawa matrices. But we envisage a high-scale SO(3)-symmetric mass spectrum

JHEP11(2022)065

for the heavy Majorana neutrinos, possibly of the order of GUT scale [22, 23], which is broken by renormalisation-group (RG) and new-physics threshold effects. Following a less constrained approach to model-building, we also assume an approximate $\mathbb{Z}_6$-symmetric texture for the entries of the neutrino Yukawa matrix. Such a construction enables the generation of the observed small neutrino masses, without imposing the expected seesaw suppression on the neutrino Yukawa parameters for heavy neutrino masses at the electroweak scale.

The layout of the paper is as follows. In section 2 we describe the minimal extension of the SM that we will be studying, and introduce the flavour structure of its leptonic Yukawa sector. In section 3 we specify the light neutrino mass spectrum for our analysis, and present the cLFV observables one may expect to probe in this model, such as $\mu \to e\gamma$, $\mu \to eee$, and coherent $\mu \to e$ conversion in nuclei. In section 4 we explore the different aspects of leptogenesis, notably the CP violation generated in RL and TRL scenarios and derive the relevant set of BEs, upon which our numerical estimates are based. This set of BEs is solved including contributions from chemical potentials while crucially preserving the temperature dependence of the key parameter, denoted later as $h_{\rm eff}(T)$, that describes the variation of the relativistic dofs with T. In section 5 we present approximate solutions to the BEs, which will help us to shed light on the attractor properties of our fully-fledged numerical estimates. In section 6 we give a summary of our numerical results, including evolution plots for the BAU and comparisons with observable quantities. Finally, section 7 summarises our conclusions and discusses possible future directions. Some technical aspects of our study have been relegated to appendices A, B and C.

2 Seesaw extension of the Standard Model

We adopt the framework of the conventional seesaw extension of the SM. This extension requires the addition of $n \geq 2$ right-handed neutrinos, which are singlets under the SM gauge group, and have lepton number $L_{\nu_R} = 1$. Given this particle content and quantum number assignments, the Lagrangian of the right-handed neutrino sector reads:

$$\mathcal{L}_{\nu_R} = i\overline{\nu}_R \not{\partial} \nu_R - \left(\overline{L}\, \mathbf{h}^{\nu} \tilde{\Phi}\, \nu_R + \frac{1}{2} \overline{\nu}_R^C\, \mathbf{m}_M \nu_R + \text{H.c.} \right). \tag{2.1}$$

Here, $L_i = (\nu_{iL}, e_{iL})^{\mathsf{T}}$, with $i = 1, 2, 3$, denote the left-handed lepton doublets, while $\nu_{\alpha R}$, with $\alpha = 1, \ldots, n$, are the right-handed neutrino fields. The matrices $\mathbf{h}^{\nu}$ and $\mathbf{m}_M$ are the neutrino Yukawa and the Majorana mass matrices, respectively, and $\tilde{\Phi}$ is the weak isospin conjugate of the Higgs doublet Φ. Note that we reserve bold face for matrices in flavour space, and assume the implicit contraction of flavour space indices.

Without loss of generality, we assume that the Majorana mass matrix is diagonal, in which case we may recast the Lagrangian eq. (2.1) in the unbroken phase as

$$\mathcal{L}_{\nu_R} = i\overline{N} \not{\partial} N - \left(\overline{L}\, \mathbf{h}^{\nu} \tilde{\Phi}\, P_R N + \text{H.c.} \right) - \frac{1}{2} \overline{N}\, \mathbf{m}_M N, \tag{2.2}$$

where $P_{R/L} = \frac{1}{2}\left(\mathbf{1}_4 \pm \gamma_5\right)$ is the right-/left- chiral projector, $\mathbf{1}_n$ is the $n \times n$ identity matrix, $\mathbf{m}_M = \text{diag}(m_{N_1}, \ldots, m_{N_n})$, and $N_\alpha = \nu_{\alpha R} + \nu_{\alpha R}^C$ are the mass-eigenstate Majorana spinors associated to the right-handed neutrinos.

JHEP11(2022)065

In the broken phase, this picture changes by the mixing between singlet and left-handed neutrinos. The mass eigenstates are particular combinations of the weak eigenstate neutrinos, given by

$$P_R \begin{pmatrix} \nu \\ N \end{pmatrix} = \begin{pmatrix} U_{\nu\nu_L^C} & U_{\nu\nu_R} \\ U_{N\nu_L^C} & U_{N\nu_R} \end{pmatrix} \begin{pmatrix} \nu_L^C \\ \nu_R \end{pmatrix} , \tag{2.3}$$

where $\nu_{1,2,3}$ are the light neutrino mass eigenstates and U is a $(3+n)\times(3+n)$ unitary matrix that diagonalises the neutrino mass matrix (see section 2.1). The subscripts, ν_L^C and ν_R, on its sub-blocks indicate the possible components of the right-handed chirality projection of each mass eigenstate, represented here as vector columns ν and N. Following the notation of [24], we may then write the Lagrangian for the charged current interaction of the heavy neutrinos as

$$\mathcal{L}_{\text{int}}^{W} = -\frac{g_w}{\sqrt{2}} W_\mu^- \overline{e}_{iL} B_{i\alpha} \gamma^\mu P_L N_\alpha + \text{H.c.} , \tag{2.4}$$

where g_w is the gauge coupling associated to the $\text{SU}(2)_L$ group, and

$$B_{i\alpha} \simeq \xi_{i\alpha} = \left(\mathbf{m}_D \mathbf{m}_M^{-1}\right)_{i\alpha} \tag{2.5}$$

is the light-to-heavy neutrino mixing at first order in the expansion of the matrix-valued parameter ξ [24]. In the following, we assume that the charged lepton Yukawa matrix is diagonal, and hence $B_{i\alpha} = (U_{\nu\nu_R})_{i\alpha}$. At first order in ξ, the effective light neutrino mass matrix, $\mathbf{m}^\nu$, follows the well-known seesaw relation [7]

$$\mathbf{m}^\nu = -\mathbf{m}_D \mathbf{m}_M^{-1} \mathbf{m}_D^{\mathsf{T}} , \tag{2.6}$$

where $\mathbf{m}_D = \mathbf{h}^\nu v/\sqrt{2}$ is the Dirac mass matrix, and $v \simeq 246\,\text{GeV}$ is the vacuum expectation value (VEV) of the Higgs field. By virtue of this relation, it is apparent that a Dirac mass matrix at a scale

$$\|\mathbf{m}_D\| \equiv \sqrt{\text{Tr}\left[\mathbf{m}_D^\dagger \mathbf{m}_D\right]} \approx v , \tag{2.7}$$

would in principle require GUT scale heavy neutrinos, which means that any impact of the singlet neutrino sector on experimental signatures would be beyond the realm of observation. This motivates the search for new model building strategies to explain sub-eV light neutrinos, whilst maintaining agreement with light neutrino data and other low energy experiments.

2.1 Neutrino flavour model

In order to explain the smallness of neutrino masses, we investigate scenarios where the neutrino mass matrix is naturally small, preferably arising from the subtle breaking of a symmetry. When this symmetry is exact, eq. (2.6) vanishes identically, given by the 3×3 null matrix, $\mathbf{0}_3$, i.e.

$$\mathbf{m}_D\, \mathbf{m}_M^{-1}\, \mathbf{m}_D^{\mathsf{T}} = \mathbf{0}_3 . \tag{2.8}$$

JHEP11(2022)065

If we consider a singlet neutrino sector with a nearly degenerate mass spectrum, this is approximately equivalent to require that prior to the breaking of the symmetry the leading Yukawa matrix, $\mathbf{h}_0^\nu$, satisfies the condition

$$\mathbf{h}_0^\nu \, \mathbf{h}_0^{\nu\mathsf{T}} = \mathbf{0}_3 \,. \tag{2.9}$$

Considering a model with three right-handed neutrinos, this motivates the following structure for the leading neutrino Yukawa matrix:

$$\mathbf{h}_0^\nu = \begin{pmatrix} a & a\,\omega & a\,\omega^2 \\ b & b\,\omega & b\,\omega^2 \\ c & c\,\omega & c\,\omega^2 \end{pmatrix} , \tag{2.10}$$

where the parameters a, b, and c are in general real, and ω is the generator of the $\mathbb{Z}_6$ group, $\omega = \exp(\pi i/3)$. We remark that this choice is not unique, and the vanishing of the light neutrino mass matrix may be realised through other constructions of the neutrino Yukawa matrix. For example, one could replace the $\mathbb{Z}_6$ element ω with the $\mathbb{Z}_3$ element $\omega' = \exp(-2\pi i/3)$. However, for concreteness, we select the $\mathbb{Z}_6$-symmetry realisation for our analysis.

Evidently, the flavour structure of eq. (2.10) has to be perturbed in order to reproduce the observed neutrino oscillation phenomenon, which requires massive neutrinos. Even though $\mathbf{h}_0^\nu$ as given by eq. (2.10) is rank one, a perturbation $\delta\mathbf{h}^\nu$ such that $\text{rank}(\delta\mathbf{h}^\nu) \geq 2$ is sufficient to explain neutrino oscillations, as long as the following condition is enforced:

$$(\mathbf{h}_0^\nu + \delta\mathbf{h}^\nu)\, \mathbf{m}_M^{-1}\, (\mathbf{h}_0^\nu + \delta\mathbf{h}^\nu)^\mathsf{T} = \frac{2}{v^2}\, \mathbf{m}^\nu \,, \tag{2.11}$$

where $\mathbf{m}^\nu$ is a 3×3 complex and symmetric matrix. Taking a, b, c, and the singlet neutrino spectrum as input parameters, eq. (2.11) defines a set of 12 constraints for the entries of the perturbation matrix $\delta\mathbf{h}^\nu$. The solutions to eq. (2.11) have to satisfy a further condition, which is $|\delta\mathbf{h}^\nu_{ij}|/|(\mathbf{h}^\nu_0)_{kl}| \ll 1$, with $i,j,k,l = 1,2,3$. More generally, the zero mass condition of eq. (2.9) can be enforced when the Majorana mass matrix $\mathbf{m}_M$ is not proportional to the identity, or even in the case when loop corrections to the tree-level seesaw relation of eq. (2.6) are considered. This gives us complete control over the loop corrections to the light-neutrino mass matrix at all orders. For example, we can incorporate one-loop corrections to $\mathbf{m}^\nu$ [24] by modifying the tree-level zero mass condition as follows [25]:

$$\mathbf{h}_0^\nu \left[\mathbf{m}_M^{-1} - \frac{\alpha_w}{16\pi M_W^2} \mathbf{m}_M^\dagger f\left(\mathbf{m}_M \mathbf{m}_M^\dagger\right) \right] \mathbf{h}_0^{\nu\mathsf{T}} = \mathbf{0}_3 \,, \tag{2.12}$$

where

$$f\left(\mathbf{m}_M \mathbf{m}_M^\dagger\right) = \frac{M_H^2}{\mathbf{m}_M \mathbf{m}_M^\dagger - M_H^2 \mathbf{1}_3} \ln\left(\frac{\mathbf{m}_M \mathbf{m}_M^\dagger}{M_H^2}\right) + \frac{3M_Z^2}{\mathbf{m}_M \mathbf{m}_M^\dagger - M_Z^2 \mathbf{1}_3} \ln\left(\frac{\mathbf{m}_M \mathbf{m}_M^\dagger}{M_Z^2}\right) . \tag{2.13}$$

In the above, $\alpha_w \equiv g_w^2/(4\pi)^2$ is the electroweak-coupling parameter, and M_W, M_Z, and M_H are the masses of the W, Z, and Higgs bosons, respectively. Redefining the quantity

JHEP11(2022)065

inside the square brackets in eq. (2.12) as an effective inverse Majorana mass, $\overline{\mathbf{m}}_M^{-1}$, the restrictions can be recast as

$$\mathbf{h}_0^\nu \overline{\mathbf{m}}_M^{-1} \mathbf{h}_0^{\nu\mathsf{T}} = \mathbf{0}_3 \,. \tag{2.14}$$

This can be further simplified by rescaling the columns of the Yukawa matrix using the definition

$$\mathbf{H}_0^\nu = \mathbf{h}_0^\nu \, \overline{\mathbf{m}}_M^{-1/2} \,, \tag{2.15}$$

which leads to

$$\mathbf{H}_0^\nu \, \mathbf{H}_0^{\nu\mathsf{T}} = \mathbf{0}_3 \,. \tag{2.16}$$

This results in the same condition of eq. (2.9) but this time for a rescaled Yukawa matrix, $\mathbf{H}_0^\nu$, with dimensions of $(\text{mass})^{-1/2}$. This shows that even for appreciable mass splittings between the singlet neutrinos and with the inclusion of loop corrections to the neutrino mass matrix, the Yukawa matrix can always be chosen in such a way that the neutrinos are massless by taking

$$\mathbf{H}_0^\nu = \begin{pmatrix} \ell_1 & \ell_1\,\omega & \ell_1\,\omega^2 \\ \ell_2 & \ell_2\,\omega & \ell_2\,\omega^2 \\ \ell_3 & \ell_3\,\omega & \ell_3\,\omega^2 \end{pmatrix} , \tag{2.17}$$

where $\ell_{1,2,3}$ are real parameters. The dimensionless Yukawa matrix, $\mathbf{h}_0^\nu$, can be found using eq. (2.15), and as explained previously, its structure can then be perturbed to reproduce the observed neutrino mass matrix $\mathbf{m}^\nu$. Here we will not address the origin of the texture of the neutrino Yukawa matrix $\mathbf{h}_0^\nu$, but it can be the subject of future studies on model building.

It is worthy to mention that the neutrino mass matrix is model dependent, and its relation to the observable parameters measured in neutrino oscillation experiments is given by

$$\mathbf{m}^\nu = U_{\text{PMNS}}^{\mathsf{T}} \, \widehat{\mathbf{m}}^\nu U_{\text{PMNS}} \,, \tag{2.18}$$

where U_{PMNS} is the PMNS lepton mixing matrix [26, 27] and $\widehat{\mathbf{m}}^\nu = \text{diag}(m_1, m_2, m_3)$, in which $m_{1,2,3}$ are the light neutrino masses. The matrix U_{PMNS} performs the Takagi factorisation [28, 29] when applied to the light neutrino mass matrix. If the Yukawa matrix of the charged leptons is assumed to be diagonal, U_{PMNS} parameterises the flavour mixing in charged current interactions of the leptonic sector. The experimental values of the parameters involved in eq. (2.18) are discussed in the next section.

3 Low energy observables

The observation of flavour neutrino oscillations at Super-Kamiokande [5] and the Sudbury Neutrino Observatory [3, 4] provides definite evidence of their massive nature. The resulting

JHEP11(2022)065

neutrino oscillation parameters offer strong constraints on the neutrino model parameters, which we discuss in this section. In addition, we present the formulae for the rates of selected charged cLFV processes, namely $\mu \to e\gamma$, $\mu \to eee$ and coherent $\mu \to e$ conversion in nuclei, which can be distinctive signatures of Majorana neutrino models, and are crucially dependent on the light-to-heavy neutrino mixing parameter presented in eq. (2.5).

3.1 Neutrino oscillation data

In order to incorporate the neutrino mass constraints into our model, we follow the procedure outlined in section 2.1. We neglect the non-unitarity effects that arise due to light-to-heavy neutrino mixing, and without loss of generality, we assume that the charged lepton Yukawa matrix, $\mathbf{h}^\ell$, is diagonal. With the first assumption in mind, the matrix $U_{\rm PMNS}$ can be parameterised as follows [30, 31]:

$$U_{\rm PMNS} = \begin{pmatrix} c_{12}c_{13} & s_{12}c_{13} & s_{13}e^{-i\delta} \\ -s_{12}c_{23} - c_{12}s_{23}s_{13}e^{i\delta} & c_{12}c_{23} - s_{12}s_{23}s_{13}e^{i\delta} & s_{23}c_{13} \\ s_{12}c_{23} - c_{12}c_{23}s_{13}e^{i\delta} & -c_{12}s_{23} - s_{12}c_{23}s_{13}e^{i\delta} & c_{23}c_{13} \end{pmatrix} \times \mathrm{diag}\left(e^{i\alpha_1/2}, e^{i\alpha_2/2}, 1\right), \tag{3.1}$$

where $c_{ij} = \cos\theta_{ij}$ and $s_{ij} = \sin\theta_{ij}$ are the cosines and sines of the neutrino mixing angles, δ is the so-called Dirac phase, and $\alpha_{1,2}$ are the Majorana phases. Together with the neutrino squared mass differences $\Delta m^2_{21} \equiv m_2^2 - m_1^2$ and $\Delta m^2_{31} \equiv m_3^2 - m_1^2$, these angles and the Dirac phase comprise the light neutrino oscillation data.

The values of these parameters are experimentally bounded with the exception of the absolute neutrino mass scale, characterised by $\min(m_{1,3})$, and the sign of $\Delta m^2_{31} \equiv m_3^2 - m_1^2$, which requires the distinction between the normal ($\Delta m^2_{31} > 0$) and inverted ($\Delta m^2_{31} < 0$) ordering hypotheses. For our numerical estimates, we use the latest best fit values for the neutrino oscillation parameters [32]:

$$\Delta m^2_{21} \equiv m_2^2 - m_1^2 = 7.50 \times 10^{-5}\,(\mathrm{eV})^2, \qquad \Delta m^2_{31} \equiv m_3^2 - m_1^2 = 2.55 \times 10^{-3}\,(\mathrm{eV})^2, \tag{3.2}$$

$$\theta_{12} = 34.3^\circ, \qquad \theta_{23} = 49.26^\circ, \qquad \theta_{13} = 8.58^\circ, \qquad \delta = 194^\circ. \tag{3.3}$$

Since the experimental data allows a massless neutrino, for definiteness we work under the hypothesis that $m_1 = 0$ and the light neutrino spectrum follows normal ordering. Likewise, for the unconstrained Majorana phases, we set $\alpha_{1,2} = 0$. For relevant tri-resonant benchmarks, we provide the relevant $\delta\mathbf{h}^\nu$ values, which reproduce the light neutrino data in appendix C.

3.2 Lepton flavour violation

In the seesaw extension of the SM, the leading order contributions to cLFV processes appear at the one-loop level [33]. For the radiative decays of our interest, the expressions for the

JHEP11(2022)065

Nucleus ($^{A}_{Z}X$)	$V^{(p)}$	$V^{(n)}$	D	Γ_{capt} (10^6 s^{-1})
$^{27}_{13}$Al	0.0161	0.0173	0.0362	13.45
$^{48}_{22}$Ti	0.0396	0.0468	0.0864	2.59
$^{197}_{79}$Au	0.0974	0.146	0.189	13.07

Table 1. Overlap integrals and muon capture rates for the nuclei of the elements used in the relevant experiments.

branching ratios are given by [34]

$$\text{BR}(\mu \to e\gamma) = \frac{\alpha_w^3 s_w^2}{256\pi^2} \frac{m_\mu^4}{M_W^4} \frac{m_\mu}{\Gamma_\mu} \left| G_\gamma^{\mu e} \right|^2 , \tag{3.4}$$

$$\begin{aligned} \text{BR}(\mu \to eee) = \frac{\alpha_w^4}{24576\pi^3} \frac{m_\mu^4}{M_W^4} \frac{m_\mu}{\Gamma_\mu} \Bigg\{ & 2 \left| \frac{1}{2} F_{\text{Box}}^{\mu eee} + F_Z^{\mu e} - 2s_w^2 \left(F_Z^{\mu e} - F_\gamma^{\mu e} \right) \right|^2 \\ & + 4s_w^4 \left| F_Z^{\mu e} - F_\gamma^{\mu e} \right|^2 + 16 s_w^2 \, \Re e \left[\left(F_Z^{\mu e} + \frac{1}{2} F_{\text{Box}}^{\mu eee} \right) G_\gamma^{\mu e *} \right] \\ & - 48 s_w^4 \, \Re e \left[\left(F_Z^{\mu e} - F_\gamma^{\mu e} \right) G_\gamma^{\mu e *} \right] + 32 s_w^4 \left| G_\gamma^{\mu e} \right|^2 \left[\ln \left(\frac{m_\mu^2}{m_e^2} \right) - \frac{11}{4} \right] \Bigg\} , \end{aligned} \tag{3.5}$$

where $s_w \equiv \sin\theta_w$ is the sine of the weak angle, m_e is the mass of the electron, and m_μ and Γ_μ are the muon mass and width. The form factors are defined in appendix B. It is worth mentioning that other cLFV decays involving τ leptons are also allowed, but we ignore them in the discussion of our results since the experimental bounds that apply to those processes are far weaker in the parameter space of interest to us.

The rate for the $\mu \to e$ conversion in an atomic nucleus $^{A}_{Z}X$ is given by [35]

$$R_{\mu\to e}^X = \frac{2G_F^2 \alpha_w^2 m_\mu^5}{16\pi^2 \Gamma_{\text{capt}}} \left| 4V^{(p)} \left(2\tilde{F}_u^{\mu e} + \tilde{F}_d^{\mu e} \right) + 4V^{(n)} \left(\tilde{F}_u^{\mu e} + 2\tilde{F}_d^{\mu e} \right) + \frac{s_w^2}{2e} G_\gamma^{\mu e} D \right|^2 , \tag{3.6}$$

where G_F is Fermi's constant, $e = g_w s_w$ is charge of the electron, Γ_{capt} is the nuclear capture rate, and $V^{(p)}, V^{(n)}, D$ are numerical estimations of the overlap integrals involved in the calculation of the conversion rate [36]. For the nuclei of our interest, table 1 presents the numerical values of these parameters. The form factors $\tilde{F}_q^{\mu e}$ ($q = u, d$) in eq. (3.6) are defined as

$$\tilde{F}_q^{\mu e} = Q_q s_w^2 F_\gamma^{\mu e} + \left(\frac{I_3^q}{2} - Q_q s_w^2 \right) F_Z^{\mu e} + \frac{1}{4} F_{\text{Box}}^{\mu eqq} , \tag{3.7}$$

where $Q_u = 2/3$, $Q_d = -1/3$ refer to the electric charges of up- and down-type quarks, and $I_3^u = 1/2$, $I_3^d = -1/2$ denote the third component of their weak isospin. The corresponding form factors can be found in appendix B.

The search for cLFV is a prominent experimental endeavour, and there are several facilities that operate with the aim of finding a conclusive hint for this class of transitions. Despite the non-observation of these signals, experimental efforts have lead to stringent

JHEP11(2022)065

bounds on the parameter space of Majorana neutrino models, which are reflected by the current upper limits

$$\begin{aligned} \mathrm{BR}(\mu \to e\gamma) &< 4.2 \times 10^{-13} && \text{MEG [18]}, \\ \mathrm{BR}(\mu \to eee) &< 1.0 \times 10^{-12} && \text{SINDRUM [37]}, \\ R^{\mathrm{Au}}_{\mu\to e} &< 7.0 \times 10^{-13} && \text{SINDRUM [38]}. \end{aligned} \tag{3.8}$$

These limits are expected to be improved by a few orders of magnitude in the near future. There is a new generation of experiments that are either starting to take data, under construction, or in the proposal/design stage. Among them, we should mention MEG-II, COMET, Mu3e, Mu2e and PRISM, with the following projected sensitivities:

$$\begin{aligned} \mathrm{BR}(\mu \to e\gamma) &< 6 \times 10^{-14} && \text{MEG II [19]}, \\ \mathrm{BR}(\mu \to eee) &< 10^{-16} && \text{Mu3e [17]}, \\ R^{\mathrm{Al}}_{\mu\to e} &< 3 \times 10^{-17} && \text{Mu2e [39]}, \\ R^{\mathrm{Al}}_{\mu\to e} &< 10^{-17} && \text{COMET [20]}, \\ R^{\mathrm{Ti}}_{\mu\to e} &< 10^{-18} && \text{PRISM [21]}. \end{aligned} \tag{3.9}$$

These projections will be compared with the cLFV rates as predicted by our leptogenesis model to assess its testability in the foreseeable future.

3.2.1 Non-zero leptonic CP phases in cLFV processes

Here we examine the impact of leptonic CP phases on cLFV processes for our class of seesaw models. It was argued in [40] that the existence of non-zero leptonic CP phases may have a substantive impact on the rate of cLFV processes through the interference terms involving the mixing $B_{\ell\alpha}$. Following a procedure similar to [40], we write the elements of $B_{i\alpha}$ as a magnitude $s_{i\alpha}$ and a phase $\varepsilon_{i\alpha}$. Thus, the terms that appear in the observable quantities are

$$\sum_{\alpha=1}^{3} B_{i\alpha}B^*_{j\alpha} = \sum_{\alpha=1}^{3} s_{i\alpha}s_{j\alpha}e^{i(\varepsilon_{i\alpha}-\varepsilon_{j\alpha})} = \sum_{\alpha=1}^{3} s_{i\alpha}s_{j\alpha}e^{i\Delta^{ij}_{\alpha}}\,, \tag{3.10}$$

where we have introduced the CP phases $\Delta^{ij}_{\alpha} = \varepsilon_{i\alpha} - \varepsilon_{j\alpha}$. These CP phases are expected to be small and can easily be extracted by taking the ratio of imaginary to real parts of the mixing, i.e.

$$\frac{\Im m\left\{B_{i\alpha}B^*_{j\alpha}\right\}}{\Re e\left\{B_{i\alpha}B^*_{j\alpha}\right\}} = \tan\left(\Delta^{ij}_{\alpha}\right) \approx \Delta^{ij}_{\alpha}\,. \tag{3.11}$$

For the model introduced in section 2, the heavy neutrino masses are nearly degenerate and the elements of the mixing matrix are all of similar scale. Therefore, the observable quantities may be approximated by taking the masses to be exactly degenerate and letting $s_{i\alpha} \approx s_{i1}$ for all α. Under these simplifications, the variations in the cLFV observables are captured in the value of

$$\left|\sum_{\alpha=1}^{3} B_{i\alpha}B^*_{j\alpha}\right|^2 \approx s^2_{i1}s^2_{j1}\sum_{\alpha,\beta=1}^{3}\cos\left(\Delta^{ij}_{\alpha} - \Delta^{ij}_{\beta}\right)\,. \tag{3.12}$$

JHEP11(2022)065

Then, the observed deviation due to the existence of non-zero leptonic CP phases may be written as

$$D^{ij} = 1 - \frac{\left|\sum_{\alpha=1}^{3} B_{i\alpha} B_{j\alpha}^{*}\right|^{2}}{\left|\sum_{\alpha=1}^{3} B_{i\alpha} B_{j\alpha}^{*}\right|^{2}_{\Delta_i=0}} \approx 1 - \frac{1}{9} \sum_{\alpha,\beta=1}^{3} \cos\left(\Delta_{\alpha}^{ij} - \Delta_{\beta}^{ij}\right) . \tag{3.13}$$

In the case of small leptonic CP phases, it can be seen that the deviation in the rate of cLFV processes away from the CP conserving rate may be given by

$$D^{ij} \approx \frac{1}{9}\left[\left(\Delta_1^{ij} - \Delta_2^{ij}\right)^2 + \left(\Delta_1^{ij} - \Delta_3^{ij}\right)^2 + \left(\Delta_2^{ij} - \Delta_3^{ij}\right)^2\right], \tag{3.14}$$

and so the observed deviation is itself a small effect.

In the context of the $\mathbb{Z}_6$ motivated model we have presented, the quantity $B_{i\alpha}B_{j\alpha}^{*}$ is completely real at lowest order, and therefore the leptonic CP phases are identically zero. Therefore, in order to have non-zero leptonic CP phases, we need to include the symmetry breaking term $\delta\mathbf{h}^{\nu}$. It is then easy to verify that up to leading order in the perturbations, $\delta\mathbf{h}^{\nu}$, the relevant leptonic CP phases are given by

$$\Delta_{\alpha}^{ij} \approx \frac{\Im m\left\{\left(\mathbf{h}_0^{\nu}\mathbf{m}_M^{-1}\right)_{i\alpha}\left(\delta\mathbf{h}^{\nu}\mathbf{m}_M^{-1}\right)^{*}_{j\alpha} + \left(\delta\mathbf{h}^{\nu}\mathbf{m}_M^{-1}\right)_{i\alpha}\left(\mathbf{h}_0^{\nu}\mathbf{m}_M^{-1}\right)^{*}_{j\alpha}\right\}}{\left(\mathbf{h}_0^{\nu}\mathbf{m}_M^{-1}\right)_{i\alpha}\left(\mathbf{h}_0^{\nu}\mathbf{m}_M^{-1}\right)^{*}_{j\alpha}} . \tag{3.15}$$

Hence, $|\Delta_{\alpha}^{ij}| \sim \|\delta\mathbf{h}^{\nu}\|/\|\mathbf{h}_0^{\nu}\| \ll 1$. We may therefore expect the deviation away from the CP conserving cLFV observables to be very small in magnitude, $D^{ij} \sim \|\delta\mathbf{h}^{\nu}\|^2/\left(9\|\mathbf{h}_0^{\nu}\|^2\right)$. For the generic scenarios listed in appendix C, one finds a deviation of $D^{ij} \sim 10^{-3}$, so any CP effect will be difficult to observe for the TRL models under study.

4 Tri-resonant leptogenesis

4.1 Leptonic asymmetries

In leptogenesis, the CP violating effects that lead to the generation of a net baryon asymmetry come from the difference between the decay rate of heavy neutrinos into Higgs and leptons, and their charge-conjugate processes. In RL models, the absorptive part of the wavefunction contribution to the decay rate [41] is central to capture the resonance effects that arise in models with nearly degenerate singlet neutrino masses, and that result in the enhancement of CP violation [42]. To facilitate the presentation of the analytic results for the CP asymmetry in heavy neutrino decays within this framework, we introduce the coefficients [13, 16]

$$A_{\alpha\beta} = \sum_{l=1}^{3} \frac{\mathbf{h}_{l\alpha}^{\nu}\mathbf{h}_{l\beta}^{\nu *}}{16\pi} = \frac{(\mathbf{h}^{\nu\dagger}\mathbf{h}^{\nu})^{*}_{\alpha\beta}}{16\pi}, \tag{4.1}$$

$$V_{l\alpha} = \sum_{k=1}^{3}\sum_{\gamma\neq\alpha} \frac{\mathbf{h}_{k\alpha}^{\nu *}\mathbf{h}_{k\gamma}^{\nu}\mathbf{h}_{l\gamma}^{\nu}}{16\pi} f\left(\frac{m_{N_\gamma}^2}{m_{N_\alpha}^2}\right), \tag{4.2}$$

JHEP11(2022)065

which pertain to the absorptive transition amplitudes for the propagator and vertex, respectively. Here $f(x) = \sqrt{x}\left[1-(1+x)\ln\left(\frac{1+x}{x}\right)\right]$ is the Fukugita-Yanagida one-loop function [11].

A full and consistent resummation of the CP-violating loop corrections, including three Majorana neutrino mixing, generates the following effective $L\tilde{\Phi}N$ Yukawa couplings [13, 16, 22]:

$$(\bar{\mathbf{h}}^{\nu}_{+})_{l\alpha} = \mathbf{h}^{\nu}_{l\alpha} + iV_{l\alpha} - i\sum_{\beta,\gamma=1}^{3}|\varepsilon_{\alpha\beta\gamma}|\,\mathbf{h}^{\nu}_{l\beta} \times \frac{m_{N_\alpha}\left(M_{\alpha\alpha\beta}+M_{\beta\beta\alpha}\right) - iR_{\alpha\gamma}\left[M_{\alpha\gamma\beta}\left(M_{\alpha\alpha\gamma}+M_{\gamma\gamma\alpha}\right)+M_{\beta\beta\gamma}\left(M_{\alpha\gamma\alpha}+M_{\gamma\alpha\gamma}\right)\right]}{m^2_{N_\alpha}-m^2_{N_\beta}+2im^2_{N_\alpha}A_{\beta\beta}+2i\,\Im m R_{\alpha\gamma}\left(m^2_{N_\alpha}|A_{\beta\gamma}|^2+m_{N_\beta}m_{N_\gamma}\Re e A^2_{\beta\gamma}\right)}\,, \tag{4.3}$$

where $\epsilon_{\alpha\beta\gamma}$ is the anti-symmetric Levi-Civita symbol, $M_{\alpha\beta\gamma} \equiv m_{N_\alpha}A_{\beta\gamma}$ and

$$R_{\alpha\beta} \equiv \frac{m^2_{N_\alpha}}{m^2_{N_\alpha}-m^2_{N_\beta}+2im^2_{N_\alpha}A_{\beta\beta}}\,. \tag{4.4}$$

The corresponding CP-conjugate effective Yukawa coupling, which is associated to the $L^C\tilde{\Phi}^*N$ interaction, is denoted by $(\bar{\mathbf{h}}^{\nu}_{-})_{l\alpha}$, and it can be found through the replacement of $\mathbf{h}^{\nu}_{l\alpha}$ with $(\mathbf{h}^{\nu}_{l\alpha})^*$ in eq. (4.3). Notably, this resummed Yukawa coupling captures all possible degrees of resonance between the contributions to the CP asymmetry from the mixing between the singlet neutrinos, which includes the *bi-resonant* and *tri-resonant* cases. We should clarify here that the bi-resonant case implies maximally enhanced CP asymmetries through the mixing of two singlet neutrinos, and the tri-resonant implies maximally enhanced CP asymmetries through the mixing of all three singlet neutrinos. Moreover, in this formalism CP violation comes from the difference between the resummed Yukawa couplings $(\bar{\mathbf{h}}^{\nu}_{-})_{l\alpha}$ and $(\bar{\mathbf{h}}^{\nu}_{+})_{l\alpha}$, as it can be seen by calculating the heavy neutrino decay rates and scattering amplitudes with the help of eq. (4.3). Note that for a model with two right-handed neutrinos (or equivalently, for a model utilising the bi-resonant approximation), the resummed Yukawa matrices are found by setting $R_{\alpha\beta}$ to zero in eq. (4.3).

Using these effective Yukawa couplings, the partial decay widths of the heavy neutrinos read

$$\Gamma(N_\alpha \to L_l\Phi) = \frac{m_{N_\alpha}}{8\pi}\left|(\bar{\mathbf{h}}^{\nu}_{+})_{l\alpha}\right|^2, \qquad \Gamma(N_\alpha \to L^C_l\Phi^\dagger) = \frac{m_{N_\alpha}}{8\pi}\left|(\bar{\mathbf{h}}^{\nu}_{-})_{l\alpha}\right|^2. \tag{4.5}$$

In turn, these decay rates can be used to find the size of the CP asymmetries for each lepton family, which for a given right-handed neutrino N_α are defined as

$$\delta_{\alpha l} \equiv \frac{\Gamma\left(N_\alpha \to L_l\Phi\right) - \Gamma\left(N_\alpha \to L^C_l\Phi^\dagger\right)}{\sum_{k=e,\mu,\tau}\Gamma\left(N_\alpha \to L_k\Phi\right)+\Gamma\left(N_\alpha \to L^C_k\Phi^\dagger\right)} = \frac{\left|\left(\bar{\mathbf{h}}^{\nu}_{+}\right)_{l\alpha}\right|^2 - \left|\left(\bar{\mathbf{h}}^{\nu}_{-}\right)_{l\alpha}\right|^2}{\left(\bar{\mathbf{h}}^{\nu\dagger}_{+}\bar{\mathbf{h}}^{\nu}_{+}\right)_{\alpha\alpha}+\left(\bar{\mathbf{h}}^{\nu\dagger}_{-}\bar{\mathbf{h}}^{\nu}_{-}\right)_{\alpha\alpha}}. \tag{4.6}$$

We also define the total CP asymmetry, δ_α, associated with each heavy neutrino species:

$$\delta_\alpha \equiv \sum_{l=e,\mu,\tau}\delta_{\alpha l}\,. \tag{4.7}$$

JHEP11(2022)065

In particular, a non-vanishing δ_α may only be generated in models, for which the flavour- and rephasing-invariant CP-odd quantity

$$\Delta_{\rm CP} = \Im m \left\{ {\rm Tr} \left[(\mathbf{h}^\nu)^\dagger \, \mathbf{h}^\nu \mathbf{m}_M^\dagger \mathbf{m}_M \mathbf{m}_M^\dagger \, (\mathbf{h}^\nu)^{\mathsf{T}} \, (\mathbf{h}^\nu)^* \, \mathbf{m}_M \right] \right\} \tag{4.8}$$

$$= \sum_{\alpha<\beta} m_{N_\alpha} m_{N_\beta} \left(m_{N_\alpha}^2 - m_{N_\beta}^2 \right) \Im m \left[\left(\mathbf{h}^{\nu\dagger} \mathbf{h}^\nu \right)^2_{\beta\alpha} \right] \tag{4.9}$$

is non-zero [12, 13, 43, 44]. For the model presented in section 2, this CP-odd quantity may be expressed as

$$\Delta_{\rm CP} \approx \left(a^2 + b^2 + c^2 \right)^2 \sum_{\alpha<\beta} m_{N_\alpha} m_{N_\beta} \left(m_{N_\alpha}^2 - m_{N_\beta}^2 \right) \Im m \left(\omega^{2(\alpha-\beta)} \right) . \tag{4.10}$$

When all heavy neutrino masses are exactly degenerate, the CP-odd invariant $\Delta_{\rm CP}$ vanishes. However, with the inclusion of mass differences, $\Delta_{\rm CP}$ is proportional to the imaginary part of the $\mathbb{Z}_6$ element ω^2 only.

Several applications of the RL formalism (e.g. [45–51]) exploit the bi-resonant enhancement of CP violating effects due to the mixing of two Majorana neutrinos, while the contribution to the CP asymmetry due a third singlet neutrino is either absent due to the neutrino mass model choice, or negligible when compared to the one generated in the decays of the resonating pair. However, in a model with three right-handed neutrinos, in the region where the masses of the heavy neutrinos satisfy the resonance condition

$$|m_{N_\alpha} - m_{N_\beta}| \simeq \frac{\Gamma_{N_{\alpha,\beta}}}{2} \qquad (\alpha \neq \beta), \tag{4.11}$$

effects of constructive interference generated by a third resonating neutrino can further enhance CP violation as compared to the case when only two neutrinos are in resonance. Figure 1 shows the behaviour of the CP asymmetries in the decays of N_1, N_2, and N_3, as well as the total CP asymmetry $\delta_T = \sum_\alpha \delta_\alpha$, plotted against m_{N_3}. In this figure, the mass of N_2 is fixed at the value $m_{N_2} = m_{N_1} + \Gamma_{N_1}/2$, therefore it fulfills the bi-resonant condition. On the left panel, it can be seen that when $m_{N_3} = m_{N_2}$, the total CP asymmetry (solid red line) vanishes due to the destructive interference effect of N_3, while at $m_{N_3} = m_{N_2} + \Gamma_{N_2}/2$, $|\delta_T|$ reaches a maximum that is more than 35% higher than in a model where the mass of the third singlet neutrino lies outside the resonance region (i.e., high m_{N_3}). In this tri-resonant point, one has $\delta_1 \approx \delta_3$, while δ_2 is the dominant contribution to δ_T. Furthermore, we find that the values of $\delta_{1,2,3}$ are independent of the mass scale, m_{N_1}, provided that the tri-resonant condition is satisfied. Thus, the enhancement of δ_2 is pervasive throughout the tri-resonant parameter space. The middle panel of figure 1 shows the impact of the proper three-neutrino mixing resummation on the asymmetry δ_2 by comparing the asymmetry calculated by considering three Majorana neutrino mixing ($\delta_2^{(3)}$) with the two-neutrino mixing case ($\delta_2^{(2)}$). When m_{N_3} lies in the resonance region, it can be seen that the mixing with N_3 becomes important, and there is a sizeable difference between the two- and three-neutrino mixing scenarios, where the latter has a sizeable enhancement effect on δ_2. The right panel of figure 1 shows that the inclusion of three-neutrino mixing also affects the size of the maximum magnitude of the asymmetry in the decays of N_3, although to a lesser extent.

JHEP11(2022)065

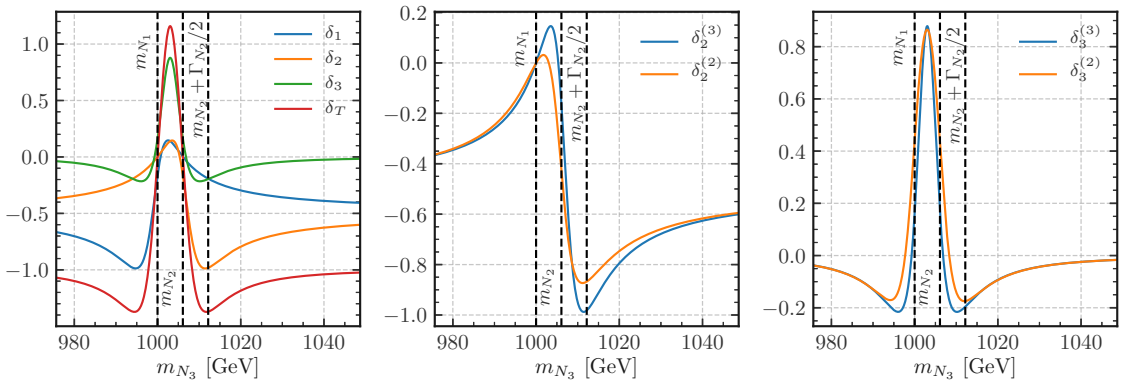

Figure 1. *Left panel:* CP asymmetries in the decays of N_1, N_2 and N_3, together with the total CP asymmetry $\delta_T = \sum_\alpha \delta_\alpha$, as a function of the mass of N_3. *Centre panel:* CP asymmetry in the decay of N_2 vs. m_{N_3} as calculated in a model that considers two-neutrino mixing ($\delta_2^{(2)}$) and three-neutrino mixing ($\delta_2^{(3)}$). *Right panel:* CP asymmetry in the decay of N_3 vs. m_{N_3} calculated in a model that considers two-neutrino mixing ($\delta_3^{(2)}$) and three-neutrino mixing ($\delta_3^{(3)}$). In all three panels, the vertical dashed lines indicate, from left to right, the values of m_{N_1}, m_{N_2} and the tri-resonant value of m_{N_3} (for details, see text).

Overall, figure 1 showcases a resonant enhancement of the total CP asymmetry of the model when the three heavy neutrinos are in successive resonance, a scenario that we have described as tri-resonant, in contrast to the bi-resonant approximation commonly studied in the literature. We identify a particular tri-resonant structure which generates appreciable BAU and maximises the scale of CP asymmetry within a model with three singlet neutrino mixing. In the literature, there also exist studies which consider the mixing effects of three singlet neutrinos [22, 23, 52–55]. These studies utilise a flavour structure different to the $\mathbb{Z}_6$ structure we have adopted, and in the case of [53], it is more similar to that proposed in [56]. Hence, the flavour structure presented in these studies cannot be mapped onto the discrete flavour symmetries we have used here, so as to enable some meaningful comparison. Finally, we must point out that our approximate $\mathbb{Z}_6$-symmetric flavour structure provides both light neutrino masses, and the origin for CP violation.

4.2 Boltzmann equations

The conditions for generating a BAU, dictated by [10], require not only a violation of the CP symmetry, but also a departure from thermal equilibrium and baryon number violation. Here, we introduce the set of Boltzmann equations that describe the out-of-equilibrium dynamical generation of a lepton asymmetry in the early Universe, and assume that it is reprocessed into a net baryon number through equilibrium $(B + L)$-violating sphaleron transitions [57].

At temperatures, T, pertinent to leptogenesis, the Universe is assumed to be radiation dominated, with an energy and entropy density given by

$$\rho(T) = \frac{\pi^2}{30} g_{\rm eff}(T)\, T^4\,, \tag{4.12}$$

$$s(T) = \frac{2\pi^2}{45} h_{\rm eff}(T)\, T^3\,, \tag{4.13}$$

JHEP11(2022)065

respectively. Here $g_{\rm eff}$ and $h_{\rm eff}$ are the relativistic dofs of the SM plasma that correspond to ρ and s, respectively. For our numerical results, we use the tabulated data[1] for the relativistic dofs as calculated in [59].[2]

The evolution of the heavy neutrino and lepton asymmetry number densities are described by their respective BEs in terms of the dimensionless parameter $z_\alpha = m_{N_\alpha}/T$, for $\alpha = 1, 2, 3$. In line with previous conventions, we use $z = z_1$. These BEs are presented in [16], and due to the approximate democratic structure of the neutrino Yukawa matrix in our TRL models, we sum over lepton flavours, which leaves us with four coupled evolution equations.

Following the conventions of [16], we normalise all number densities with the photon number density

$$n_\gamma(z_\alpha) = \frac{2\zeta(3)T^3}{\pi^2} = \frac{2\zeta(3)}{\pi^2}\left(\frac{m_{N_\alpha}}{z_\alpha}\right)^3, \tag{4.14}$$

which for a given particle species i, gives us the ratio

$$\eta_i(z_\alpha) = \frac{n_i(z_\alpha)}{n_\gamma(z_\alpha)}\,. \tag{4.15}$$

In addition, we define the departure from equilibrium for the heavy-neutrino density as

$$\delta\eta_{N_\alpha}(z_\alpha) = \frac{\eta_{N_\alpha}(z_\alpha)}{\eta^{\rm eq}_{N_\alpha}(z_\alpha)} - 1\,, \tag{4.16}$$

where $\eta^{\rm eq}_{N_\alpha}$ denotes η_{N_α} in thermal equilibrium, for which we use the approximate expression

$$\eta^{\rm eq}_{N_\alpha}(z_\alpha) \approx \frac{z_\alpha^2}{2\zeta(3)} K_2(z_\alpha). \tag{4.17}$$

Here, $\zeta(3) \approx 1.202$ is Apéry's constant, and $K_n(z)$ is a modified Bessel function of the second kind. In the BEs, we have also included terms which depend on the parameter

$$\delta_h(z_\alpha) = 1 - \frac{1}{3}\frac{d\ln h_{\rm eff}}{d\ln z_\alpha}\,, \tag{4.18}$$

since we allow $h_{\rm eff}$ to vary with T.[3]

Considering decay terms, $\Delta L = 1$ and $\Delta L = 2$ scattering processes, and the running of the dof parameters, the BEs can be written as[4]

$$\begin{aligned}\frac{d\delta\eta_{N_\alpha}}{d\ln z_\alpha} =& -\frac{\delta_h(z_\alpha)}{H(z_\alpha)\;\eta^{\rm eq}_{N_\alpha}(z_\alpha)}\left[\delta\eta_{N_\alpha}\left(\Gamma^{D(\alpha)}+\Gamma_Y^{S(\alpha)}+\Gamma_G^{S(\alpha)}\right)+\frac{2}{9}\,\eta_L\,\delta_\alpha\left(\tilde\Gamma^{D(\alpha)}+\hat\Gamma_Y^{S(\alpha)}+\hat\Gamma_G^{S(\alpha)}\right)\right]\\ &+(\delta\eta_{N_\alpha}+1)\left[z_\alpha\frac{K_1(z_\alpha)}{K_2(z_\alpha)}-3\left(\delta_h(z_\alpha)-1\right)\right],\end{aligned} \tag{4.19}$$

[1] We have extracted the corresponding data file from the source code of `MicrOMEGAs` [58].

[2] From [59] we choose the equation of state model labeled as C.

[3] In fact, in the data file we have extracted from `MicrOMEGAs`, the relativistic dofs are not constant even at temperatures well above 100 GeV. This unexpected behaviour arises from combined lattice [60] and perturbative QCD [61] considerations to the equation of state of the plasma, leading to deviations from the ideal gas assumption at high temperatures [59].

[4] In order to solve the system of equations eqs. (4.19) and (4.20), we employ the implementation of `RODASPR2` [62] provided in `NaBBODES` [63]. We have checked that other methods [64, 65] as well as the ones provided by `scipy` [66] produce the same results. The relativistic dofs of the plasma are interpolated using `SimpleSplines` [67] and the various integrals needed for the collision terms are evaluated using `LAInt` [68]. Finally, all figures are made using the versatile visualization library `matplotlib` [69].

JHEP11(2022)065

$$\frac{d\eta_L}{d\ln z} = -\frac{\delta_h(z)}{H(z)}\Bigg\{\sum_{\alpha=1}^{3}\delta\eta_{N_\alpha}\delta_\alpha\left(\Gamma^{D(\alpha)}+\Gamma_Y^{S(\alpha)}+\Gamma_G^{S(\alpha)}\right) + \frac{2}{9}\eta_L\left[\sum_{\alpha=1}^{3}\left(\tilde{\Gamma}^{D(\alpha)}+\tilde{\Gamma}_Y^{S(\alpha)}+\tilde{\Gamma}_G^{S(\alpha)}+\Gamma_Y^{W(\alpha)}+\Gamma_G^{W(\alpha)}\right)+\Gamma^{\Delta L=2}\right] + \frac{2}{27}\eta_L\sum_{\alpha=1}^{3}\delta_\alpha^2\left(\Gamma_Y^{W(\alpha)}+\Gamma_G^{W(\alpha)}\right)\Bigg\} - 3\eta_L\left(\delta_h(z)-1\right), \tag{4.20}$$

where

$$H(z_\alpha) = \sqrt{\frac{4\pi^3 g_{\rm eff}(z_\alpha)}{45}}\frac{m_{N_\alpha}^2}{M_{\rm Pl}}\frac{1}{z_\alpha^2} \tag{4.21}$$

is the Hubble parameter, and $M_{\rm Pl}\approx 1.221\times 10^{19}\,\text{GeV}$ is the Planck mass. Since the BEs are not identical to the ones utilised in the literature due to the non-trivial T-dependence of $h_{\rm eff}$, we show how they are obtained in appendix A. The various collision terms are defined in the literature [16] as

$$\Gamma^{D(\alpha)} = \frac{1}{n_\gamma}\gamma_{L\Phi}^{N_\alpha}, \tag{4.22}$$

$$\tilde{\Gamma}^{D(\alpha)} = \left(1+\frac{12}{21}\right)\Gamma^{D(\alpha)}, \tag{4.23}$$

$$\Gamma_Y^{S(\alpha)} = \frac{1}{n_\gamma}\left[\gamma_{Qu^C}^{N_\alpha L}+2\gamma_{LQ^C}^{N_\alpha u^C}\right], \tag{4.24}$$

$$\tilde{\Gamma}_Y^{S(\alpha)} = \frac{1}{n_\gamma}\left[\left(\delta\eta_{N_\alpha}+1+\frac{12}{21}\right)\gamma_{Qu^C}^{N_\alpha L}+\left(2+\frac{98}{159}(\delta\eta_{N_\alpha}+2)\right)\gamma_{LQ^C}^{N_\alpha u^C}\right], \tag{4.25}$$

$$\hat{\Gamma}_Y^{S(\alpha)} = \frac{1}{n_\gamma}\left[\left(-(\delta\eta_{N_\alpha}+1)+\frac{12}{21}\right)\gamma_{Qu^C}^{N_\alpha L}+\left(2-\frac{98}{159}\delta\eta_{N_\alpha}\right)\gamma_{LQ^C}^{N_\alpha u^C}\right], \tag{4.26}$$

$$\Gamma_G^{S(\alpha)} = \frac{1}{n_\gamma}\left[\gamma_{L\Phi}^{N_\alpha V_\mu}+\gamma_{V_\mu\Phi^\dagger}^{N_\alpha L}+\gamma_{LV_\mu}^{N_\alpha\Phi^\dagger}\right], \tag{4.27}$$

$$\tilde{\Gamma}_G^{S(\alpha)} = \frac{1}{n_\gamma}\left[\left(1+\frac{12}{21}\right)\gamma_{L\Phi}^{N_\alpha V_\mu}+\left(\delta\eta_{N_\alpha}+1+\frac{12}{21}\right)\gamma_{V_\mu\Phi^\dagger}^{N_\alpha L}+\left(1+(\delta\eta_{N_\alpha}+1)\frac{12}{21}\right)\gamma_{LV_\mu}^{N_\alpha\Phi^\dagger}\right], \tag{4.28}$$

$$\hat{\Gamma}_G^{S(\alpha)} = \frac{1}{n_\gamma}\left[\left(1+\frac{12}{21}\right)\gamma_{L\Phi}^{N_\alpha V_\mu}+\left(-(\delta\eta_{N_\alpha}+1)+\frac{12}{21}\right)\gamma_{V_\mu\Phi^\dagger}^{N_\alpha L}+\left(1-(\delta\eta_{N_\alpha}+1)\frac{12}{21}\right)\gamma_{LV_\mu}^{N_\alpha\Phi^\dagger}\right], \tag{4.29}$$

$$\Gamma_Y^{W(\alpha)} = \frac{1}{n_\gamma}\left[\left(2+\frac{12}{21}\right)\gamma_{Qu^C}^{N_\alpha L}+\left(2+\frac{12}{7}\right)\gamma_{LQ^C}^{N_\alpha u^C}\right], \tag{4.30}$$

$$\Gamma_G^{W(\alpha)} = \frac{1}{n_\gamma}\left[\left(1+\frac{12}{21}\right)\gamma_{L\Phi}^{N_\alpha V_\mu}+\left(2+\frac{12}{21}\right)\gamma_{V_\mu\Phi^\dagger}^{N_\alpha L}+\left(1+\frac{24}{21}\right)\gamma_{LV_\mu}^{N_\alpha\Phi^\dagger}\right], \tag{4.31}$$

$$\Gamma^{\Delta L=2} = \frac{2}{n_\gamma}\left(1+\frac{12}{21}\right)\left[\gamma'^{L\Phi}_{L^C\Phi^\dagger}+\gamma_{\Phi^\dagger\Phi^\dagger}^{LL}\right], \tag{4.32}$$

where γ_Y^X are CP-conserving collision terms for the process $X\to Y$. The latter is defined as

$$\gamma_Y^X \equiv \gamma\left(X\to Y\right)+\gamma\left(\overline{X}\to\overline{Y}\right), \tag{4.33}$$

JHEP11(2022)065

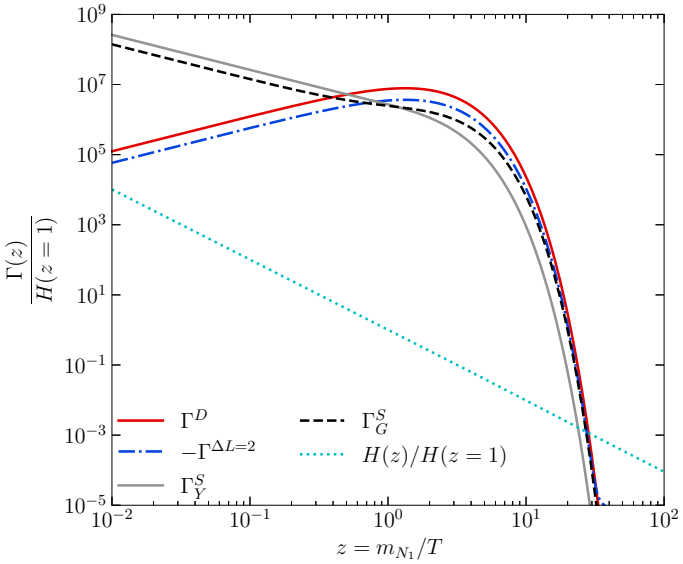

Figure 2. The $\delta\eta_{N_\alpha}$ independent collision terms are defined in (4.32) for $|\mathbf{h}^\nu_{ij}| \approx 3 \times 10^{-3}$ and $m_{N_1} = 500\,\text{GeV}$. The wash-out terms, $\Gamma^W_{Y,G}$, are uniformly different by a factor of two compared to their source ($\Gamma^S_{Y,G}$) counterparts.

where the bar denotes CP conjugation. The pertinent analytical expressions of the collision terms and scattering cross sections can all be found in [16].[5] Note that the primed terms correspond to collision terms with subtracted real intermediate states (RIS), which can take negative values due to the lack of an on-shell contribution to the squared amplitude.

The typical dependence of the various collision terms on $z = m_{N_1}/T$ is shown in figure 2, for $|\mathbf{h}^\nu_{ij}| \approx 3 \times 10^{-3}$ and $m_{N_1} = 500\,\text{GeV}$. The other two masses obey the tri-resonant condition, which results in a sizeable $\Delta L = 2$ rate. It is noteworthy that the collision term that describes the decays and the RIS parts is larger than $\Gamma^{\Delta L=2}$, as also observed in [13]. For this figure, the relevant perturbation matrix, $\delta\mathbf{h}^\nu$, needed to match the neutrino data may be found in appendix C under Benchmark **A**.

During leptogenesis, part of the lepton asymmetry that is generated in the processes described above is partially converted into a baryon asymmetry by $(B + L)$-violating sphaleron transitions which become exponentially suppressed below the temperature $T_{\text{sph}} \simeq 132\,\text{GeV}$ [71]. In order to compare the generated BAU at $T = T_{\text{sph}}$ to its value at the recombination epoch, we assume that there are no considerable entropy releasing processes, and hence the entropy density remains approximately constant as the Universe cools. Using entropy conservation and the relation $s(T) \sim h_{\text{eff}}(T)\, T^3$, it can be shown that the BAU at T_{sph} is related to the BAU at T_{rec} by

$$\eta_B^{\text{rec}} = \frac{h_{\text{eff}}(T_{\text{rec}})}{h_{\text{eff}}(T_{\text{sph}})} \frac{n_B(T_{\text{sph}})}{n_\gamma(T_{\text{sph}})} = f \frac{n_B(T_{\text{sph}})}{n_\gamma(T_{\text{sph}})}\,. \tag{4.34}$$

[5] For the gauge and Yukawa mediated cross section, we use the lepton thermal mass, as infra-red regulator [70].

JHEP11(2022)065

For the dilution factor, f, we use the approximate value 1/27 [13, 72], while for the conversion factor between lepton and baryon number above the sphaleron temperature, we use the equilibrium relation given by [73]

$$\eta_B = -\frac{28}{51}\eta_L \,. \tag{4.35}$$

5 Approximate solutions to Boltzmann equations

In this section we discuss the solution of the BEs eqs. (4.19) and (4.20) in order to understand the production of a lepton asymmetry in the early Universe. As a first approach, we consider a simplified version of these equations, where we ignore the "back-reaction" (i.e. the second term of eq. (4.19)), the variation of the relativistic dofs, and only take into account the decay and RIS terms. Moreover, we assume that $m_{N_1} \approx m_{N_2} \approx m_{N_3}$.

5.1 Approximation for $\delta\eta_{N_\alpha}$

We begin by solving the equation for $\delta\eta_{N_\alpha}$, which takes the form

$$\frac{d\delta\eta_{N_\alpha}}{dz} = \frac{K_1(z)}{K_2(z)}\left[1 + \left(1 - z\frac{\Gamma_{N_\alpha}}{H(z=1)}\right)\,\delta\eta_{N_\alpha}\right] . \tag{5.1}$$

Initially (at $z \ll 1$), right-handed neutrinos are taken to be in thermal equilibrium, so $\delta\eta_{N_\alpha} = 0$. Therefore, at early times, we expect the second term of eq. (5.1) to vanish. Moreover, at such high temperatures, we may approximate $K_1(z)/K_2(z) \approx z/2$, so

$$\delta\eta_{N_\alpha} \approx \frac{z^2}{4}\,, \qquad \text{for } z \ll 1\,. \tag{5.2}$$

As the temperature drops, $\delta\eta_{N_\alpha}$ increases, and at some point the second term starts to become comparable to the first. So, $\delta\eta_{N_\alpha}$ continues to increase until both terms become equal. We denote this point as $z = \hat{z}$, and assuming $\hat{z} \gg H(z=1)/\Gamma_{N_\alpha}$, it is estimated as

$$\hat{z} \approx \left(\frac{4\,H(z=1)}{\Gamma_{N_\alpha}}\right)^{1/3} . \tag{5.3}$$

For $z \approx \hat{z}$, we observe that the r.h.s. of eq. (5.1) stays close to zero. That is, $\delta\eta_{N_\alpha} \approx H(z=1)/\Gamma_{N_\alpha} z^{-1}$, since any increase (decrease) with respect to this behaviour pushes $\delta\eta_{N_\alpha}$ to negative (positive) values. Consequently, we find that for $z \gg \hat{z}$,

$$\delta\eta_{N_\alpha} \approx \frac{H(z=1)}{\Gamma_{N_\alpha} z}\,. \tag{5.4}$$

Notice that this result does not depend on the initial condition. Also, we should point out that at late times, namely $z \gg 1$, eq. (5.4) solves eq. (5.1) up to terms $\mathcal{O}(1/z^2)$.

5.1.1 The neutrino Boltzmann equation as an autonomous system

The independence from the initial conditions has been previously highlighted in the literature (e.g. [16, 22]). However, it would be helpful to analyse its attractor properties. We begin by noting that eq. (5.1) can be written in the form of an autonomous system

$$\frac{d\mathbf{r}}{dt} = \mathbf{V}\left(z(t), \delta\eta_{N_\alpha}(t)\right)\,, \tag{5.5}$$

Figure 3. The solution of (5.1) for $\Gamma_{N_\alpha} = 100\ H(z=1)$ with initial conditions $\delta\eta_{N_\alpha}(z \to 0) = 0$ (black) and $\delta\eta_{N_\alpha}(z \to 0) = 1$ (dashed red). The arrows show the direction of $\mathbf{V}$, while the colour gradient encodes the size of $\delta\eta_{N_\alpha}$, with light grey (black) for low (high) values of $|d\delta\eta_{N_\alpha}/dz|$. The vertical grey line shows the value of $\hat{z}$ as estimated by (5.3).

with $\mathbf{r} = (z, \delta\eta_{N_\alpha})^\mathsf{T}$ and

$$\mathbf{V}\left(z(t), \delta\eta_{N_\alpha}(t)\right) = \begin{pmatrix} 1 \\ \dfrac{K_1(z(t))}{K_2(z(t))}\left[1 + \left(1 - z(t)\dfrac{\Gamma_{N_\alpha}}{H(z=1)}\right)\ \delta\eta_{N_\alpha}(t)\right] \end{pmatrix}. \tag{5.6}$$

Here, the vector field $\mathbf{V}$ represents the flow of eq. (5.1), which helps to demonstrate how $\mathbf{r}$ reaches the stable solution, independently of the initial conditions. In figure 3, we show the evolution of $\delta\eta_{N_\alpha}$ for $\Gamma_{N_\alpha} = 100\, H(z=1)$ and for two different initial conditions. Along with the two curves, we show the direction of $\mathbf{V}$, which indicates at each point the tendency of $\mathbf{r}$. Moreover, darker arrows imply higher values of $|d\delta\eta_{N_\alpha}/dz|$. As both curves merge at $z \gtrsim \hat{z}$, $\delta\eta_{N_\alpha}$ ends up becoming ignorant of the initial condition. This feature is also imprinted in the direction of $\mathbf{V}$. The normalised vector, $\mathbf{V}$, is parallel to the z-axis for $z \lesssim \hat{z}$, while it points towards the solution for $z \gtrsim \hat{z}$.

5.2 Approximation for η_L

The corresponding equation for the lepton asymmetry, assuming that $\delta\eta_{N_\alpha} \sim 1/z$, can be written as

$$\frac{d\eta_L}{dz} = \frac{\delta_T}{2\zeta(3)} K_1(z)\, z^2\ \left(1 - z\,\frac{2k_L}{3\delta_T}\eta_L\right), \tag{5.7}$$

where $\delta_T = \sum_\alpha \delta_\alpha$ and $k_L = \displaystyle\sum_a \frac{\Gamma_{N_\alpha}}{H(z=1)}$.